STUDIA UBB CHEMIA, LVI, 4, 2011 (p. 97 - 106)

MICROSTRUCTURE AND PROPERTIES OF ELECTROTECHNICAL PORCELAIN

MARIA GOREA[a,*], RODICA CREŢ[b], FERENC KRISTALY[c]

ABSTRACT. We have investigated the microstructure of an industrial porcelain for medium voltage electrical insulators by the means of X-ray diffraction (XRD), as well as optical and electron (SEM) microscopy. Syn–orthorhombic mullite ($Al_{4.54}Si_{1.46}O_{9.73}$), hexagonal quartz ($SiO_2$), syn–rhombohedral corundum (Al_2O_3) and tetragonal silica (SiO_2) are the crystalline components, as determined by XRD. Electron microscopy (SEM) coupled with energy-dispersive spectroscopy (EDS) evidenced the presence of mullite crystals with variable Si:Al ratios, from 1:1, 1:2 to 1:3 or even 1:4 in the areas where K^+ is present. Small prismatic crystals were observed on the corundum grains; their composition resembles Al-rich mullite. Locally, the glass phase is highly enriched in K^+ as a result of orthoclase melt. The large quartz grains show marginal reaction rims related to the chemical attack of the feldspar melt. The physical, electric and mechanic characteristics of the porcelain vary in broad limits in direct connection with the compositional heterogeneity.

Keywords: *microstructure, porcelain, characteristics*

INTRODUCTION

Traditional vitreous ceramics such as porcelains, some refractory material and structural clay products in which significant fluid phase (30-70 %) forms during firing is obtained from a mix of kaolin, flux and filler. They were studied in detail by many authors [1-4]. Clays (usually kaolin) represent about 50 % from the mix; in the raw state they build a matrix for the other components, while during forming they confer plasticity to the ceramic body. The flux (feldspar) is included in amounts of about 25 % of the mix. It provides fluid phase at relatively low temperatures that interact with other components, leading to the formation of a melt which vitrifies the body. The filler (sand, or alumina), representing 25 %, is a stable component at high temperatures that

[a] Babeş-Bolyai University, Faculty of Chemistry and Chemical Engineering, 11 Arany Janos Str, RO-400084, Cluj-Napoca, Romania, * *mgorea@chem.ubbcluj.ro*
[b] Technical University, Faculty of Electrical Engineering, 26-28 G. Bariţiu Str. RO-400027, Cluj Napoca, Romania, rodica_cret@yahoo.fr
[c] University of Miskolc, Faculty of Earth Science and Engineering, 3515 Miskolc-Egyetemváros, Miskolc, Hungary, kristalyf81@yahoo.com

helps minimising deformation and shrinkage during firing. The last stages of the evolution of the porcelain microstructure are known only in basic lines. Mullite represents the only stable component in the Al_2O_3–SiO_2 system under normal temperatures and pressures. Pure mullite is a solid solution with Al_2 $[Al_{2+2x}\,Si_{\,2-2x}]\,O_{10-x}$ compositions, where $0.17 \leq x \leq 0.5$ [5, 6]. Mullite formation is determined by the nature of the raw materials, processing method, temperature but also the additional ingredients used for enhancing specific properties. Based on the crystallization pattern and the crystal size, two types of mullite crystals were identified in porcelains. The small mullite aggregates (< 0.5 μm) of cubic symmetry resulted from the transformation of clay minerals are called "*primary mullite*", while the long, acicular mullite (> 1 μm) noticed in the feldspar melt are called "*secondary mullite*". The Al_2O_3/SiO_2 ratio for the primary mullite is close to 2:1 (Al_2O_3-rich), while the value reaches 3:2 for secondary mullite; the Al_2O_3 content varies from the areas with clay relics to that with feldspar relics [7-11]. In the first stages of sintering the tri-component porcelains kaolin clay shrinks and cracks. Subsequently, at 500–600 ˚C, the kaolinite dehydroxylates to form metakaolinite. At around 900 ˚C it transforms into spinel, while at 1000 ˚C the fine primary mullite crystals form. Primary mullite turns into secondary mullite at high temperatures, of about 1400 ˚C. The liquid phase obtained from the melting of the feldspars at low temperatures (1100 ˚C) reacts with the components of the ceramic body, thus leading to the crystallization of the acicular secondary mullite. The latter cross-cuts the microstructure and creates a more dense body. The feldspar melting process starts at the contact areas between feldspar crystals and clay relics, the amorphous silica resulted from kaolinite decomposition being easily mobilized in the melt, at around 985 ˚C. Potential extraneous phases contained by kaolin and feldspar (Na_2O, CaO, MgO, TiO_2 or Fe_2O_3) may influence the mullite crystallization, the porcelain's vitrification temperature, and the viscosity of the melt. Quartz or alumina are refractory materials that are added into the ceramic composition for minimising the ceramic body's deformation and shrinkage, in the case of formation of significant amounts of melted phase. Quartz is structurally transformed at 573 ˚C and is considered relatively insoluble in the feldspar melt under 1250 ˚C. Above this temperature, solubilisation of quartz is evidenced by the presence of reaction rims at the contact of quartz grains with the embedding Si-rich melt. Solubilisation is controlled by the size of the grains: below 20 μm, a complete solubilisation is registered at temperatures above 1350 ˚C. The final microstructure of porcelain is built by mullite crystals, vitreous phase and small amounts of quartz surrounded by fine cracks that will define the porcelain's properties [12].

The increase in density, homogeneity degree of the ceramic body and the shrinkage mechanisms during firing are revealed when studying microstructure evolution. Such studies are of high interest for commercial porcelain industry.

Our study aims is characterizing and quantifying the mineral and amorphous phases in a particular, “aluminous”-rich electrotechnical porcelain, as well as its physical-chemical, electrical and mechanical characterization. Finally, we have correlated the material’s composition with its properties.

REZULTS AND DISCUSSIONS

Porcelain microstructure

The tested ceramic bodies are samples of commercial porcelain obtained from a mix of 50 % kaolin, 28 % feldspars and 22 % alumina processed by the wet method and submitted to thermal treatment at 1300 ˚C.

The chemical composition of the fired porcelain (Table1) is characterised by a high content of Al_2O_3 that is typical for this type of material. Also, the dominance of K_2O over Na_2O favours the formation of a viscous melt and prevents deformations upon firing; last but not least, this feature confers a higher dielectric rigidity.

Table 1. Chemical composition of the studied porcelain

Oxide	SiO_2	Al_2O_3	CaO	MgO	Na_2O	K_2O	Fe_2O_3	LOI
[%]	44.17	43.60	1.23	0.24	1.46	2.32	1.30	5.68

The phase composition of the fired porcelain was investigated by the means of XRD (figure 1), optical and electron (SEM) microscopy. The qualitative and semi-quantitative data point to the presence of about 50 to 60 % vitreous phases, which embeds the crystalline phases.

The crystalline phases mainly consist of orthorhombic synthetic mullite ($Al_{4.54}Si_{1.46}O_{9.73}$) – 54.60 %; rhombohedral synthetic corundum (Al_2O_3) – 16.60 %; hexagonal quartz (SiO_2) ~ 18.18 % and tetragonal silica dioxide (SiO_2) – 10.80 %. The unit cell parameters of these mineral components are presented in Table 2.

Table 2. The unit cell parameters of the crystalline phases

	a	b	c
Mullite (orthorhombic)	7.5421	7.6957	2.88362
Quartz (hexagonal)	4.9	4.9	5.4
Corundum (rhombohedral)	4.7607	4.7607	12.995
Silica dioxide (tetragonal)	4.978	4.978	6.9321

Mullite is an X-ray discernible crystalline compound resulted by the transformation of clayey raw materials (primary mullite), or by crystallization from feldspar melts (secondary mullite), respectively. Corundum, the high temperature Al_2O_3 phase originates from the raw materials, *i.e.* technical alumina that is not structurally transformed in the range of the firing temperature.

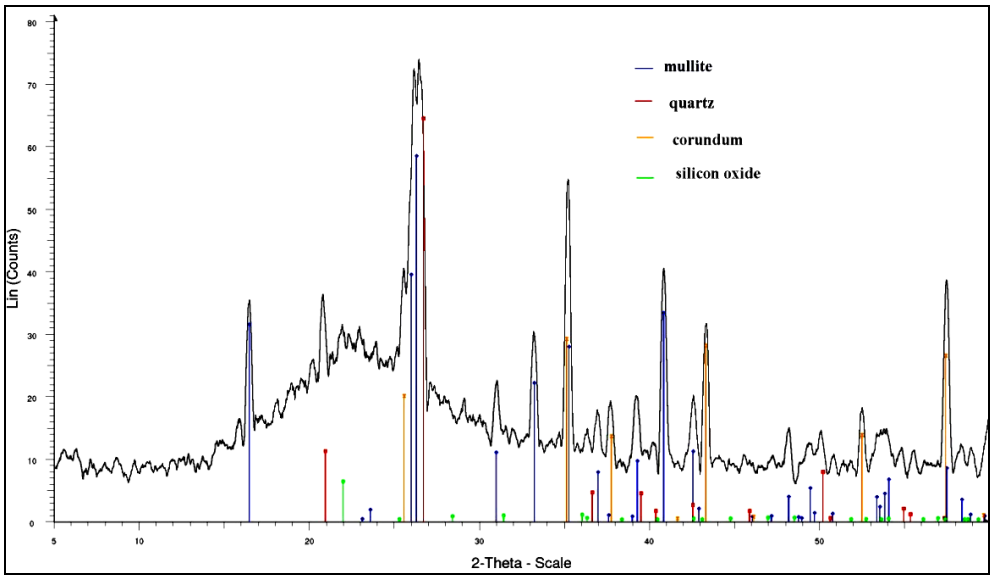

Figure 1. X-ray pattern of the electrotechnical porcelain

Hexagonal quartz, the undesirable form in electrotechnical porcelain given its volume variation during the polymorphous transition at 573 ˚C is the result of using SiO_2-rich (quartzitic) feldspar as flux raw material. Tetragonal silica dioxide represents the low temperature polymorph of cristobalite formed by clay minerals' transformations under thermal treatment (high cristobalite has cubic symmetry).

The fine texture of the porcelain is illustrated in polarizing optical microscopy images (figure 2). A high amount of quartz and closed pores within a relatively homogeneous vitreous matrix can be noticed.

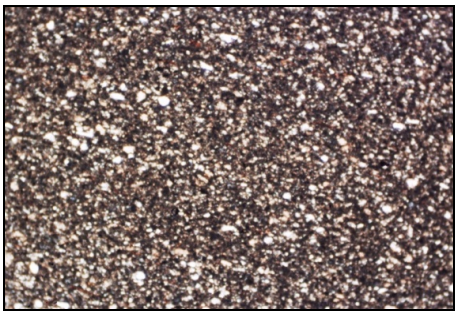

Figure 2. Electrotechnical porcelain with fine texture consisting of one vitreous and one crystalline phase; quartz is the dominant phase (1N)

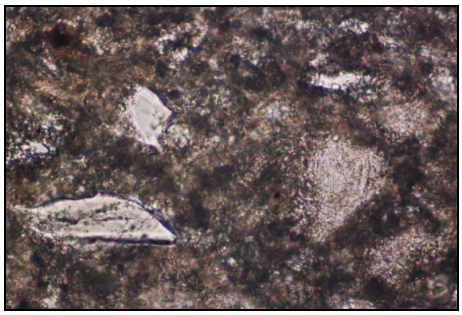

Figure 3. Quartz grains with reaction rim Fine from the interaction with the feldspar melt (1N)

The smaller quartz grains are turned into solution, while the larger ones are only partly solubilised, with the formation of a reaction rim around these particles (figure 3). The melt is rich in SiO_2, thus favouring the crystallization of the acicular secondary mullite. In some areas the melt still preserved the shape of the solubilised feldspar grain; the framework of acicular secondary mullite is well-defined, with largely crystallized outlines.

The SEM image (figure 4) of the feldspar melt evidences corundum segregations; they are probably due to an incomplete homogenization. Also only partly solubilised large quartz grains, as well as a large, unmelted orthoclase grain are also visible.

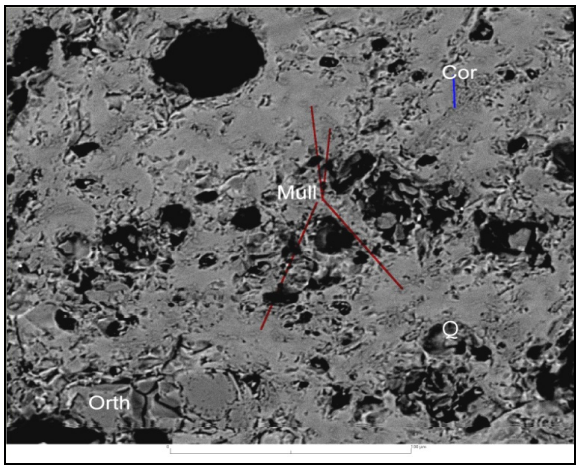

Figure 4. SEM image of the studied porcelain showing regions of mullite (Mull), corundum (cor), quartz grain (Q) and unmelted feldspar (Orth)

The transformations under firing of the clay minerals with the formation of primary mullite are documented by the SEM+EDS analyses (figure 5). The light grey areas with a 2:1 Si:Al ratio are typical for the incipient stage of transformation (and represent relics of the clay minerals). Subsequently, in the darker areas, K^+ ion is depleted, while the Si:Al ratio increases from 1:1 to 1:2, with the formation of γ-Al_2O_3 spinel. The detailed image on the right shows small crystals embedded in the vitreous matrix. In these areas, alumina is the dominant component, the Si:Al ratio varying from ~ 1:3 to 1:4. Thus, three distinctive types of mullite-containing compositions are evidenced by the SEM images: clay minerals relics with aggregates of primary mullite; clay relics cross-cut by the feldspar melt, with secondary mullite; and, an alumina-rich composition with the so-called tertiary mullite, a typical phase for Al-rich porcelains. The vitreous matrix shows a similar composition in all these investigated areas.

To summarize, electron microscopy (SEM+EDS) evidences areas with distinctive chemical compositions, starting with SiO_2-rich ones containing also alkalis (K^+) and evolving into alumina-rich ones containing To summarize, electron microscopy (SEM+EDS) evidences areas with distinctive chemical compositions, starting with SiO_2-rich ones containing also alkalis (K^+) and evolving into alumina-rich ones containing secondary mullite. In the corundum-rich areas, small prismatic crystals are assigned to the Al_2O_3-rich tertiary mullite.

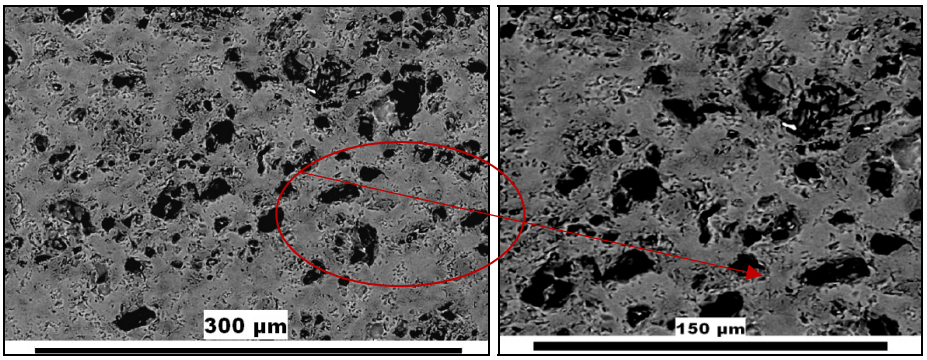

Figure 5. Microstructure of the porcelain. SEM+EDS images document areas with distinctive Al:Si compositions.

Density and apparent porosity

Compactness characteristics, as well as bending resistance are the significant physical characteristics that correlate with the microstructure of ceramics. Thus, in the case of the studied porcelain, we measured the average apparent density (ρ_a) by using the Archimedes method. The obtained value, 2.52276 g/cm^3, falls within the requested interval. On the other hand, the apparent porosity (P_a) is slightly higher, 0.11823 %, as compared to the standard value, *i.e.*, 0.0 %. Porosity – especially the one of the closed pores was also evaluated by microscopic methods; as expected, the values are relatively higher.

Electrical characterisation

The relative permittivity, the dielectric loss factor - measured at 20 °C and 100 Hz, and the volume resistivity - measured under direct current, show values within the required intervals (Table 3). Samples 1 and 3 represent exceptions; their permittivity values are slightly above the upper limit (6-7); the same is true for the loss factor of sample 4 that is somewhat higher than the standard. On the contrary, the dielectric rigidity shows lower values than the requested ones: from E_{str} > 20 MV/m they decrease even to 15-16 MV/m. This fact can be explained by the presence of some extraneous ions, as well as by the large volume of closed pores and some local compositional heterogeneities in the ceramic body.

The variation of the permittivity coefficient with temperature, $\alpha_\varepsilon(T) = 1/\ \varepsilon_{ri} \cdot \Delta\varepsilon/\Delta T$ [K^{-1}], are presented in table 4, while the variation plot in figure 6. The slope of the curve defines an experimental value $\alpha_\varepsilon(T) = 1.45 \times 10^{-3}$ [K^{-1}] that is much higher than the required one, $\alpha_\varepsilon(T) = 0.5 - 0.6 \times 10^{-3}$ [K^{-1}]. The high permittivity values can be also correlated with the high internal porosity and the presence of some impurities.

Table 3. Electrical characteristics of the studied porcelain

Sample	Relative permittivity (ε_r)	Dielectric loss factor, at 20 °C (tg δ)	Volume resistivity [Ωcm]
1.	7.17	0.023	
2.	6.33	0.019	
3.	7.10	0.022	5.8×10^{13}
4.	6.61	0.029	4.4×10^{14}
5.	6.99	0.023	
6.	6.90	0.014	
7.	6.45	0.021	8.88×10^{13}
8.	6.98	0.020	6.67×10^{13}
9.	6.80	0.014	2.2×10^{14}
standard	6-7	0.025	$> 10^{11}$

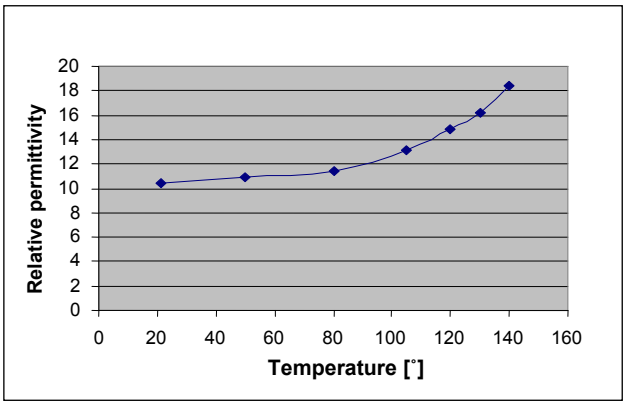

Figure 6. Variation of relative permittivity with temperature

Table 4. ε_r and $\alpha_\varepsilon(T)$ values measured at various temperatures

T [°C]	ε_r	$\alpha_\varepsilon 10^3$ [K^{-1}]
21	$\varepsilon_{ri} = 10.48$	
50	10.92	1.45
80	11.35	1.42
105	13.10	2.98
120	14.88	4.79
130	16.16	4.85
140	18.35	6.28

Mechanical characterisation

The bending resistance of the glazed porcelain, τ_g, is 147.103 MPa while that of the non-glazed one is 108.988 MPa. Both values are much higher than the standard limits, *i.e.* minimum 60 MPa and respectively minimum 50 MPa. The explanation is related to the absence of fine fissures in the ceramic body.

The mechanical compression strength was measured on 10 mm diameter cylindrical test samples of variable length by using an up-to-date universal equipment with automatic data processing and display (including $\sigma \rightarrow \varepsilon$ diagrams). The curves plotted for samples 3 and 4 are presented in figure 7.

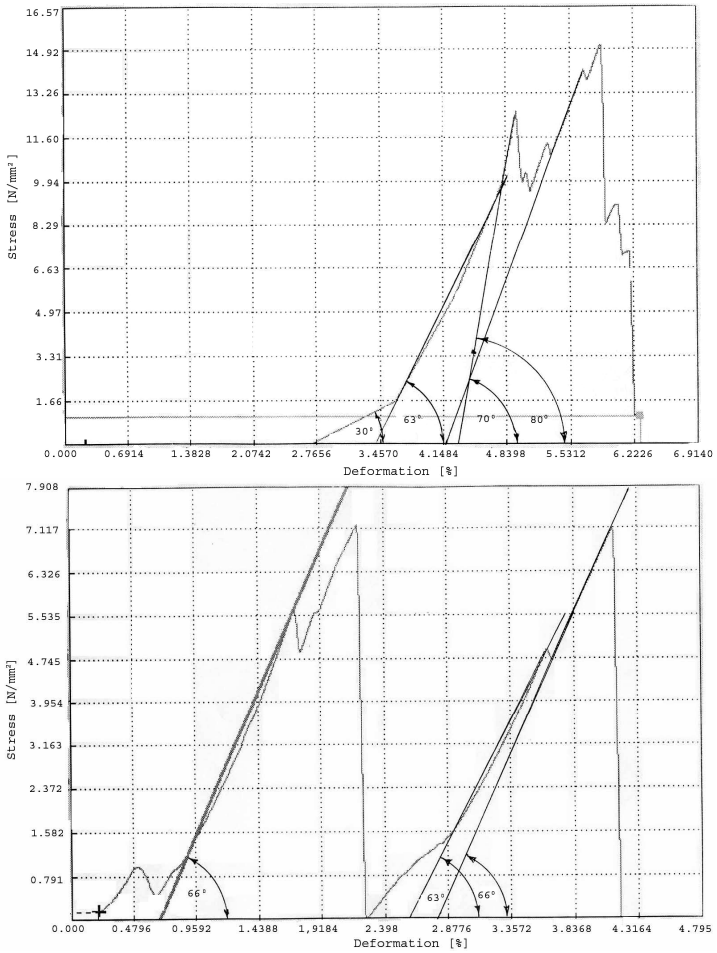

Figura 7. Tension, σ – specific linear deformation, ε diagram for tester no. 3 (left) and 4 (right) obtained by using the "Gabaldini-Sun5" equipment with automatic data processing and display

It is remarkable that the ceramic samples do not collapse in a single step; in the case of sample 3 there are four steps, while for sample 4 there are three. From the plots one can calculate β angle, which is used to determine the elasticity modulus, E. Table 5 shows the mechanical compression strength values for the porcelain test samples.

Table 5. Mechanical resistance values for the tested porcelain samples

Sample	D [mm]	$A = \pi d^2/4$ [mm]	L [mm]	Fmax [N]	$\sigma_r = Fmax/A$ [N/mm^2]	$E = tg\beta = \sigma_r/\varepsilon$ [N/mm^2]	Obs. β [°]
3	9.5	70.882	9.4	1068	15.07	1.66/0.00864 = 192	30
						9.9/0.018398= 538	63
						12.43/0.00691 = 1798.8	70
						15.07/0.0167 = 902.39	80
4	9.5	70.882	11.6	509.55	7.19	5.6/0.01059 = 528.8	66
						4.82/0.01 = 482	63
						7.117/0.0138 = 515.8	66

The breaking compression strength and the elasticity modulus values cover a wide interval for samples formed from the same material. This confirms the compositional heterogeneity of the studied porcelain.

CONCLUSIONS

The microstructural investigation of the porcelain ceramic body has evidenced the presence of heterogeneous mixtures consisting of feldspar, quartz and alumina, accompanied by insulated or aggregated particles of totally or partly transformed kaolinite. Hexagonal quartz is related to the quartzitic (SiO_2-rich) feldspar used as flux material. Feldspars are partly solubilised, as indicated by the reaction rims surrounding the grains. Tetragonal SiO_2 represents the low temperature polymorph of cristobalite resulted by thermally-induced transformations of clay minerals. Electron microscopy (SEM+EDS) evidenced the presence of areas with distinctive chemical composition, starting from SiO_2-rich ones, also containing K^+ (feldspar melt), varying to alumina-rich ones including small secondary mullite crystals. The electrical characteristics (dielectric permittivity, loss factor, volume resistivity, rigidity) vary in a large range (some beyond the acceptable limits). This can be explained by the large compositional and structural heterogeneity of the material, as well as by the presence of closed and open pores. The degree of loss is high, and it increases with increasing temperature (permittivity variation coefficient is about three times higher than the standard accepted one). The test samples show large limits of variation for the breaking compression strength and the elasticity module. These represent consequences of the compositional heterogeneity evidenced by microscopic investigation.

EXPERIMENTAL SECTION

The industrial electrotechnical porcelain samples thermally treated at 1300 ˚C have been obtained in the laboratory and then investigated by specific methods. The composition was determined by wet chemical analysis in solution. The phase composition was investigated by X-ray diffraction by using a Bruker D8 diffractometer with Cu anticathode, in the 5–64 2θ˚ interval. Optical microscopic study in polarised light was carried out on thin sections (25-30 microns) using a Nikon Eclipse E 2000 microscope, while electron microscopy (SEM+EDS) on a JEOL JXA-8600 Superprobe micro-beam electron microscope. The compaction measurements were acquired by weighting in air and water, based on the Archimedes principle. The electrical and mechanical characteristics were obtained according to the current standard procedures.

REFERENCES

1. Y. Iqbal, W.E. Lee, *J. Am. Ceram. Soc.*, **1999**, *82*[12], 3584.
2. Sujeong Lee, Youn Yoong Kim, Hi-Soo Moon*, J. Am. Ceram. Soc.,* **1999**, *82*[10], 2841.
3. H. Schneider, J. Schreuer, B. Hildman, *Journal of the European Ceramic Society*, **2008**, *28*, 329.
4. W.E. Lee, G.P. Souza, C.J. McConville, T. Tarvornpanich, Y. Iqbal, *Journal of the European Ceramic Society*, **2008**, *28*, 2, 465.
5. B.R. Johnson, W.M. Kriven, J. Schneider, *Journal of the European Ceramic Society,* **2001**, *21*, 2541.
6. S. Freimann, S. Rahman, *Journal of the European Ceramic Society,* **2001**, *21*, 2453.
7. W.E. Lee, Y. Iqbal, *Journal of the European Ceramic Society,* **2001**, *21*, 2583.
8. M.A. Sainz, F.J. Serrano, J.M. Amigo, J. Bastida, A. Caballero, *Journal of the European Ceramic Society,* **2000**, *20*, 403.
9. N. Montoya, F.J. Serrano, M.M. Reventos, J.M. Amigo, J. Alarcon, *Journal of the European Ceramic Society,* **2010**, *30*, 839.
10. Yamuna, S. Devanarayanan, M. Lalithambika, *J. Am. Ceram. Soc.*, **2002**, *85*[6], 1409.
11. S. Lee, Y.J. Kim, H.J. Lee, H.S. Moon, *J. Am. Ceram. Soc.,* **1999**, *82*[10], 2841.
12. Y. Iqbal, W.E. Lee, *J. Am. Ceram. Soc.,* **2000**, *83*[12], 3121.